Electrochimica Acta 201 (2016) 96–105

Contents lists available at ScienceDirect

Electrochimica Acta

journal homepage: www.elsevier.com/locate/electacta

From environmental pollutant to activated carbons for high-performance supercapacitors

Jiao Yin[a,b], Yunqing Zhu[a,b], Xiu Yue[a,b], Lan Wang[a,b], Hui Zhu[c,d,*], Chuanyi Wang[a,b,**]

[a] Key Laboratory of Functional Materials and Devices for Special Environments, Xinjiang Technical Institute of Physics & Chemistry, Chinese Academy of Sciences, 40-1 South Beijing Road, Urumqi, Xinjiang 830011, China
[b] Laboratory of Eco-Materials and Sustainable Technology (LEMST), Xinjiang Technical Institute of Physics & Chemistry, Chinese Academy of Sciences, 40-1 South Beijing Road, Urumqi, Xinjiang 830011, China
[c] College of Chemistry/Institute of Polymers, Nanchang University, 999 Xuefu Avenue, Nanchang 330031, China
[d] Jiangxi Provincial Key Laboratory of New Energy Chemistry, Nanchang University, 999 Xuefu Avenue, Nanchang 330031, China

ARTICLE INFO

Article history:
Received 12 February 2016
Received in revised form 31 March 2016
Accepted 31 March 2016
Available online 1 April 2016

Keywords:
environmental pollutant
methylene blue
activated carbons
supercapacitors

ABSTRACT

In this research, Methylene blue (MB), a type of environmental pollutants (dye), was initially adopted as a carbonaceous precursor to synthesize activated carbons (ACs) with the activation of $ZnCl_2$ at high temperatures. Varieties of techniques have been used to characterize the MB-derived ACs. The pore structures and surface functional groups were fully studied by N_2 adsorption-desorption analysis, XPS, IR, SEM and TEM, respectively. The MB-derived ACs have as large specific surface area as up to 2151.92 m^2g^{-1} and the pore size distribution concentrates on 2–5 nm. Moreover, electrochemical techniques such as cyclic voltammetry (CV), electrochemical impedance spectroscopy (EIS) and galvanostatic charge/discharge (GCD) were employed to assess AC's capacitive behavior and rate performance. It demonstrated that MB-derived ACs possessed as high specific capacitance as 265 Fg^{-1} at a scan rate of 5 mV s^{-1} in 1 M H_2SO_4. In addition, the MB-derived ACs exhibited long-term cycling stability and more than 90% original capacity have been maintained after first 1000 cycles (the total cycles of 10000 were carried out.) at a high current density of 1 A g^{-1}.

1. Introduction

Environmental pollutant management has been considered as a challengeable problem all over the world and some of environmental protection related research institutes in many countries have made great efforts to recycle or reutilize these pollutants. From the viewpoint of pollutant's chemical composition, most of pollutants are rich in carbon. If some natural or man-made pollutants can be appropriately reutilized as carbon precursors and transformed into diverse forms of carbons with active target functions, we could achieve high value-added products for various and flourishing carbon-based applications. Among these forms of carbon, highly porous activated carbons (ACs) possess large surface area, adjustable pore size, high conductivity, stable physical and chemical inertness. On the basis of above-mentioned advantages, highly porous ACs have been widely applied in various fields such as environment protection, medicine, food, chemical engineering, especially a highly demand in energy storage devices-supercapacitors [1–7].

Up to now, only a narrow portion of pollutants have been adopted as the precursors for preparation of supercapacitor-used ACs including human hair [8], tobacco stems [9], coal liquefaction residue [10], oil sands fluid coke [11], cow dung [12], waste tea leaves [13], bacteria [14], animal's bones and feather [15], fungi [16], dead leaves [17]. Compared with above-mentioned pollutants, a variety of dyes utilized in industries including paper-making, printing, textile, food, and pharmaceuticals are more harmful to environment and human beings. More seriously, some are even cancerogenic, teratogenetic or mutagenic, hence, it is extremely necessary to handle them in safe ways before their release to our environment [18].

Methylene blue (MB,$C_{16}H_{18}ClN_3S$), as a typical dye widely used in industry, has been considered as a common environmental pollution probe to characterize photo-catalyst performance due to the fact that MB is a common dye and difficult to be degraded [19]. However, from the viewpoint of carbon content, MB is a rich source of carbon and nitrogen. If MB is utilized as carbonaceous precursor to prepare electronically active functional types of ACs, on the one hand, the environmental pollutant has been effectively disposed,

* Corresponding author. Tel.:+ 86 431 85262063 fax: 86 431 85262063.
** Corresponding author. Tel.:+ 86 991 3835879 fax: 86 991 3835879.
E-mail addresses: huizhu@ncu.edu.cn (H. Zhu), cywang@ms.xjb.ac.cn (C. Wang).

http://dx.doi.org/10.1016/j.electacta.2016.03.196
0013-4686/

on the other hand, the more valuable product has been obtained and can be applied in electrochemical energy storage devices-supercapacitors.

Supercapacitors (SCs), also known as electrochemical capacitors, have gradually aroused more and more concern due to their merits of good power performance, satisfactory coulombic efficiency and desirable cycling life [20,21]. Up to now, various of electrochemical active materials have been proposed and applied as SC's electrode materials. Among them, ACs are considered as one of the most promising candidates for SCs because of its highly porous structures, large surface area that promotes charge collection and transfer at the electrode|electrolyte interface [22–24]. To pursue highly developed pore structure and large surface area, the activation methods and activation agents are two other important factors that influence the pore and surface area properties besides the carbon precursors [22–25]. In general, both physical and chemical activation methods are commonly used to prepare ACs [26]. The physical activation refers to the use of gasifying agents such as carbon dioxide, air or steam at high temperatures (800–1200 °C) to create porosity in carbonaceous materials [27]. However, the physical activation is time-consuming and the obtained specific surface area of carbon is too small to meet the critical requirement of capacitors. By contrary, the chemical activation is generally carried out at relatively low temperatures (600–900 °C) with the aid of chemical agents such as KOH, $ZnCl_2$ and H_3PO_4. The activation time is shorter than that of physical activation. More important, highly developed pore structure and large surface area can be achieved from chemical activation, which plays very decisive role in improving capacitor's performance [28,29]. Among the various chemical activating agents, zinc chloride ($ZnCl_2$) is milder. Furthermore, $ZnCl_2$ activation can generate well-developed pores and achieve high carbon yield due to the fact that $ZnCl_2$ often behaves as a dehydrating agent promising more carbon content to be maintained in resultant ACs, especially for small molecule carbonaceous precursors like MB [30].

Consequently, in this work, MB and $ZnCl_2$ was respectively adopted as the carbonaceous precursor and activating agent for synthesis of ACs. The merits of this facile method consist in easy operation, satisfactory reproducibility, high yield and massive production. Varieties of measurements such as N_2 adsorption-desorption, transmission electron microscopy (TEM) and Scanning electron microscopy (SEM) were employed to study the textural properties of these MB-derived ACs. Furthermore, Fourier transform-infrared (FT-IR) spectra and X-Ray photoelectron spectroscopy (XPS) were adopted to investigate the elements and surface groups of MB-derived ACs. In addition, electrochemical techniques such as cyclic voltammetry (CV), electrochemical impedance spectroscopy (EIS) and galvanostatic charge/discharge (GCD) were carried to assess their capacitive properties in the electrolyte of acid (H_2SO_4) aqueous solutions. The electrochemical characterization implied that the prepared ACs demonstrated the specific capacitance as high as 265 Fg^{-1} at a scan rate of 5 $mV\,s^{-1}$ in 1 M H_2SO_4. Moreover, supercapacitors based on MB-derived ACs exhibited long-term cycling stability in which the 90% original capacitance have been maintained even after 10000 cycles at a high current density of 1 $A\,g^{-1}$.

2. Experiments

2.1. Preparation of MB-derived ACs

As a very easy preparation method, MB (Tianjing guangfu chemical Co. Ltd.) and activating agent $ZnCl_2$ were fully mixed with weight ratio of 1:4 (MB:$ZnCl_2$). After sufficient milling, the mixture placed in quartz boat was put in tube furnace under nitrogen protection with a heating rate of 5 °C/min from room temperature to 600, 700, 800, 900 and 1000 °C, respectively. Then the $ZnCl_2$ activation process was carried out at 600–1000 °C for 1 hour. Finally, the resultant product was respectively washed by 2 M HCl and distilled water to remove impurities. The as-prepared AC samples were respectively named as $MBAC_1$ (600 °C), $MBAC_2$ (700 °C), $MBAC_3$ (800 °C), $MBAC_4$ (900 °C) and $MBAC_5$ (1000 °C) according to different activation temperatures.

2.2. Characterization of MB-derived ACs

Nitrogen adsorption-desorption isotherms were carried out by Quadrachrome adsorption instrument at 77 K. Prior to analysis, the samples were degassed under vacuum for 24 h at the temperature of 200 °C. The surface area was calculated according to the Brunauer-Emmett-Teller (BET) method. The type of FEI Tecnai G2 F20 transmission electron microscope with an acceleration

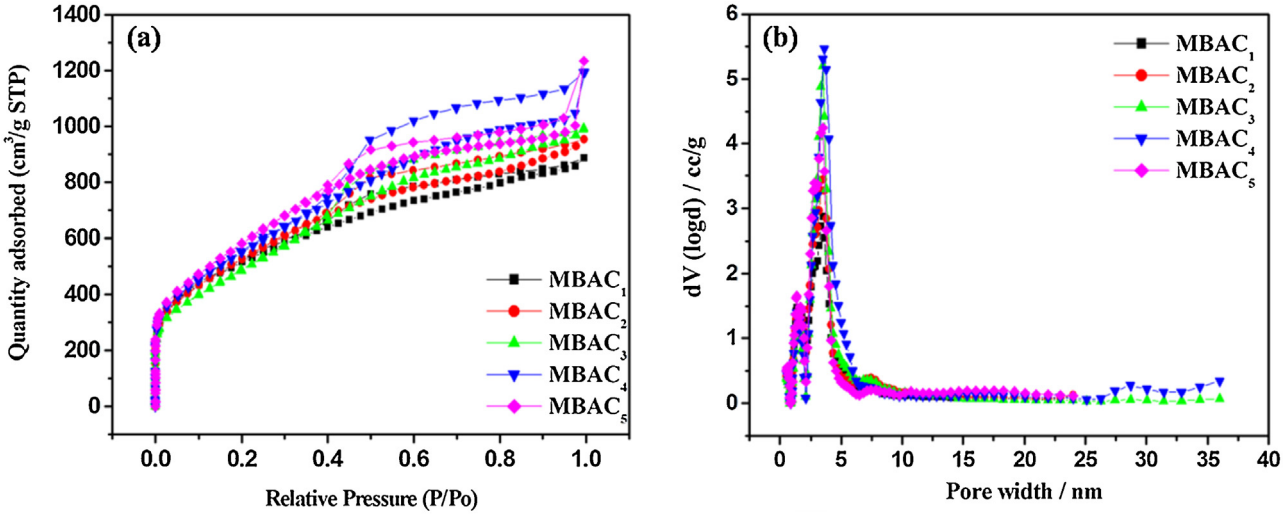

Fig. 1. N_2 adsorption/desorption analysis of MBACs (a). PSD for N_2 (b).

voltage of 200 kV was used to record the TEM and HRTEM images. The Philips XL 30 instrument and a JEOL JSM-6700F microscope were adopted to take SEM images. An ESCALAB 250 (Thermo Electron) was employed to obtain sample's XPS information. The X-ray excitation was offered by a monochromatic Al Kα (1486.6 eV) source. The avantage program was applied to quantify data. The Bruker Vertex 70 FT-IR spectrometer was utilized to record FT-IR spectra. Furthermore, the Vario EL cube (Elementar Analysensysteme GmbH) was applied to analyze elements including carbon, hydrogen, oxygen, nitrogen and sulfur.

2.3. Electrode preparation and electrochemical measurements

Electrodes in the form of films were fabricated by mixing 85 wt.% of MBACs, 10 wt.% carbon black (SUPER-P, TIMCAL) and 5 wt.% of polytetrafluoroethylene (PTFE, ALDRICH). Then the mixed films covered on stainless steel mesh was used as working electrode in which the weight of active material reached to 6 mg. Moreover, Maxsorb, a type of commercial microporous carbon (purchased from Kansai Coke and Chemicals company, Japan), was also used as electrode material to compare with MB-derived ACs.

All the CV experiments were conducted in a three-electrode system operated on an electrochemical working station (CHI660E, Shanghai, China). In this electrochemical system, the platinum foil was employed as the counter electrode, the $Hg/HgSO_4$ electrode was taken as the reference electrode. The potential window was ranged from −0.8 to +0.4 V in the acid electrolyte (1 M H_2SO_4).

EIS technique was performed on an electrochemical workstation (Zahner Im6ex) and the frequency was ranged from 100 kHz to 10 mHz with an ac signal amplitude of 5 mV at open circuit potential.

GCD experiments were carried out by a Land Battery test System (Land, PR China) and the charging-discharging current densities were ranged from 0.2 to 2 A g^{-1}.

3. Results and discussion

3.1. Porous texture characterization

Fig. 1 depicts nitrogen adsorption-desorption isotherms and pore size distribution (PSD) curves of $MBAC_1$, $MBAC_2$, $MBAC_3$, $MBAC_4$ and $MBAC_5$. All the isotherms in Fig. 1(a) for MBACs have similar shapes and belong to typical type IV isotherm. The hysteresis loop at high relative pressure ranged from 0.4 to 0.9 implies the presence of a large number of mesopores, meanwhile, some adsorbed quantity can be obviously observed at low pressure (below 0.1), indicating the presence of micropores in the system [31–33]. Furthermore, the PSD curves exhibited in Fig. 1(b) reveal that all the samples have narrow pore distribution and the pore size mainly concentrates on 2–5 nm. It also implies that PSD shows no remarkable changes with the increase of activation temperature from 600 to 1000 °C. Moreover, Table 1 describes the features of porous structure in MBACs according to the corresponding nitrogen adsorption/desorption isotherms and contrast their performance with commercial microporous Maxsorb. The specific surface area is enlarged from 1820.659 to 2151.916 m^2g^{-1} at the temperature interval of 600–1000 °C and meanwhile the average pore diameter is also gradually broadened from 3.024 to 3.600 nm. It is obviously observed that the surface area of micro-pores is remarkably reduced from 600 to 800 °C and reappear with little content at the activation temperatures of 900 and 1000 °C. On the other hand, the surface area of meso-pores is gradually enhanced from 600 to 1000 °C, however, the increase step becomes very sluggish from 900 to 1000 °C. The pore formation and development concept of $ZnCl_2$ activation leads to the above variation tendency of surface area and pore size [34]. In this activation process, on the one hand, the $ZnCl_2$ generally acts as dehydration, denitrification and desulfuration agent, which results in removal of nitrogen and sulfur groups from benzene ring and promotion of carbonization and aromatization of carbon framework, on the other hand, the $ZnCl_2$ also behaves as template in which the occupied spaces by $ZnCl_2$ will be vacated in the washing process to form pores [35]. When the activation temperature is raised, the simultaneous occurrence of broadening and collapsing of pores gives rise to the modification and shift of the specific surface area and pore size distribution.

As for electrode material of supercapacitor, micro- and meso-porous composite structure with large surface area can be considered as desirable candidate to improve both specific capacitance and rate performance. Consequently, the capacitive behavior of all samples will be investigated in detail in the next study.

3.2. Microstructure characterization of MBACs

The micro-structure of MBACs was investigated by TEM and high resolution TEM. TEM and HRTEM images displayed in Fig. 2(a–e) and (f) further illustrate that MBACs are rich in a highly meso-porous structure. The morphology of all MBACs manifest the analogous structure, as is provided in Fig. 2.

3.3. Element analysis and surface chemistry characterization of MBACs

Table 2 lists the chemical composition of the original MB and MBACs, respectively. It can be observed that the element of C experiences a sharp increase and the elements of O and N go through a rapid decrease as MB was treated in the process of

Table 1
Textural properties of MBACs.

Textural property	S_{BET}[a)] [m^2g^{-1}]	S_{micro}[b)] [m^2g^{-1}]	S_{meso}[c)] [m^2g^{-1}]	V_{total}[d)] [cm^3g^{-1}]	V_{micro}[e)] [cm^3g^{-1}]	V_{meso}[f)] [cm^3g^{-1}]	Average pore diameter (nm)
$MBAC_1$	1820.659	506.942	1313.717	1.376	0.237	1.139	3.024
$MBAC_2$	1921.591	320.478	1601.113	1. 479	0.133	1.346	3.078
$MBAC_3$	1804.641	–	1804.641	1.537	–	–	3.407
$MBAC_4$	2015.300	85.105	1930.195	1.849	0.018	1.831	3.670
$MBAC_5$	2151.916	151.783	2000.133	1.807	0.043	1.764	3.600
Maxsorb	1333.73	1080.35	236.38	0.666	0.551	0.115	2.016

[a] Specific surface area from multiple BET method (calculated in the linear P/P_0 range from 0.05 to 0.3).
[b] Micropore surface area from t-plot method.
[c] t-method external surface area ($S_{meso} = S_{BET} - S_{micro}$).
[d] Total pore volume at $P/P_0 = 0.99$.
[e] Micropore pore volume from t-plot method micropore analysis.
[f] $V_{meso} = V_{total} - V_{micro}$.

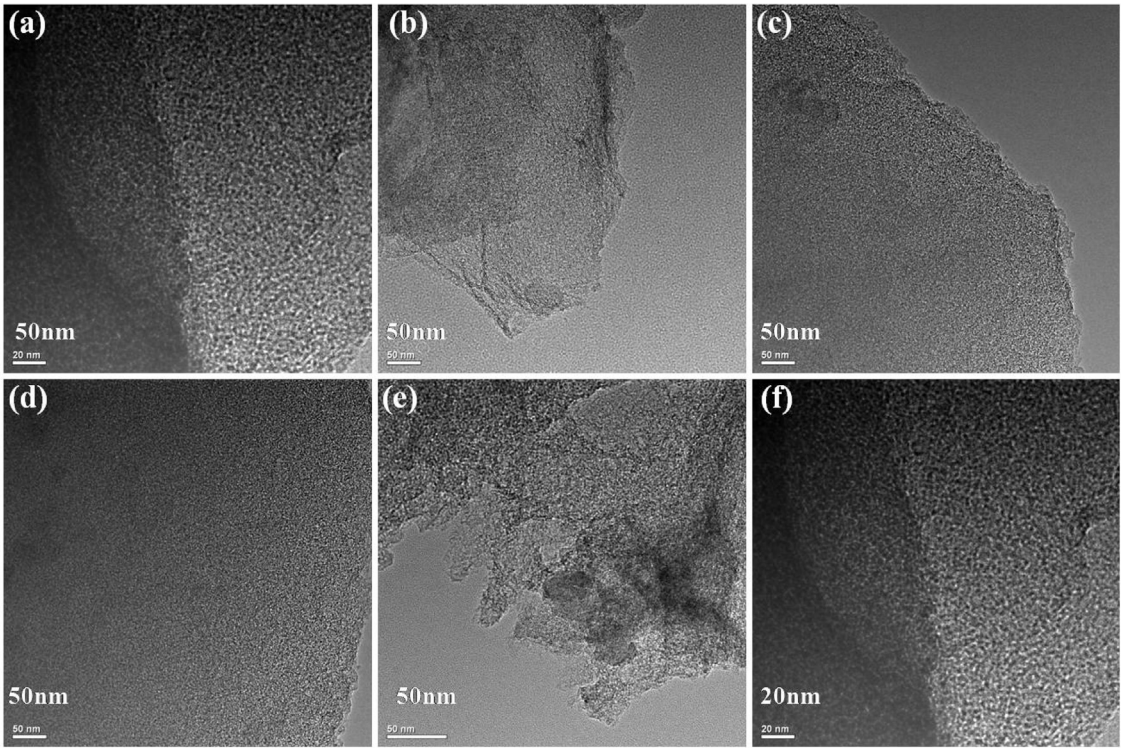

Fig. 2. TEM images of $MBAC_1$ (a), $MBAC_2$ (b), $MBAC_3$ (c), $MBAC_4$ (d), $MBAC_5$ (e) and high resolution TEM image of $MBAC_2$ (f).

carbonization and activation at high temperatures. The FT-IR spectrum of all MBACs is presented in Fig. 3(a). The peaks located at about 3420, 1597, 1200 and 1100 cm^{-1} respectively may belong to O—H stretching vibration (3420 cm^{-1}), C=C or C=O stretching vibration (1597 cm^{-1}), C—O—C or C—O stretching modes (1200 and 1100 cm^{-1}) [13,36,37]. To further accurately illuminate the composition and surface groups of MBACs, XPS measurements were performed. The deconvolution C1s XPS of all samples are exhibited in Fig. 3(b–f). The peaks located at 284.6, 286.4, 287.7, and 289.7 eV, are respectively owing to C=C—C, C—O, C=O and O—C=O groups [9,38–40]. The content of C—O, C=O and O—C=O groups are as high as 24.05%, 11.47% and 1.59% in MBAC sample, $MBAC_2$ possesses the highest content of C—O (24.05%) and C=O (11.47%) groups, $MBAC_5$ possesses the highest content of O—C=O (1.59%) group. In conclusion, the FT-IR and XPS characterizations affirm the presence of oxygen functional groups on the surface of prepared carbons, N and S atoms were not doped into carbon framework.

3.4. Electrochemical characterization

Cyclic voltammetry (CV), as an effective electrochemical technique, is usually adopted to appraise the capacitive behavior of electrode materials for supercapacitors [41]. The CVs of all MBACs displayed in Fig. 4(a–e) compare their specific capacitance and rate performance. All the CVs are measured in the three-electrode cell system, respectively, recorded at a variety of scan rates. The calculation method of specific capacitance (SC) in CV curves shown in Fig. 4(a–e) is based on the Eq. (1) [42]:

$$SC = Q/V = I/(\upsilon \times m) \quad (1)$$

herein, υ stands for the scan rate, m represents the mass of active material. The calculation method of SC in Fig. 4(f) is obtained by the Eq. (2) [43,44]:

$$SC = \frac{Q}{2 \times \Delta V \times m} \quad (2)$$

herein, Q/2 means the half of the integration area of the CV curve, V represents the total potential range, and m stands for the mass of active material in a working electrode. It can be deduced that the $MBAC_2$ displays the highest SC value (as high as 265 Fg^{-1}) at low scan rates, the $MBAC_4$ and $MBAC_5$ demonstrate better rate performance. The good capacitive response of $MBAC_2$ in acid electrolyte originates from the combination of electrical double layer capacitance (EDLC) and pseudo-capacitance respectively caused by its large surface area, well-developed pores and certain amount of oxygen functional groups. The high rate performance of $MBAC_4$ and $MBAC_5$ in acid electrolyte derives from their larger pore size compared with other three samples. The above results are according with their CV figure shape and pseudo-capacitive functional groups investigated by FTIR and XPS measurements. In summary, the CV experiments illustrate that MB-derived porous carbons manifest desirable EDLC performance in acid aqueous electrolyte, combining with remarkable pseudo-capacitance.

Furthermore, EIS technique was also carried out for all MBAC electrodes in acid electrolytes. The Nyquist plots for all carbon electrodes are exhibited in Fig. 5(a). The frequency intervals in

Table 2
The chemical composition of MBACs.

Samples	At%[a] C	At%[a] O	At%[a] N	At%[a] S	Molar Composition[b]
MB	–	–	–	–	$C_{16}H_{18}ClN_3S{\cdot}H_2O$
$MBAC_1$	73.27	23.47	3.20	0.10	$C_1H_{0.47}O_{0.37}N_{0.11}S_{0.017}$
$MBAC_2$	74.50	21.20	3.80	0.50	$C_1H_{0.31}O_{0.32}N_{0.080}S_{0.013}$
$MBAC_3$	83.50	13.00	3.50	–	$C_1H_{0.21}O_{0.26}N_{0.060}S_{0.007}$
$MBAC_4$	85.80	11.60	2.60	–	$C_1H_{0.15}O_{0.19}N_{0.019}S_{0.005}$
$MBAC_5$	89.00	8.45	2.55	–	$C_1H_{0.16}O_{0.18}N_{0.015}S_{0.007}$

[a] Atomic ratio (AT) data obtained by XPS analysis.
[b] Data obtained by element analysis.

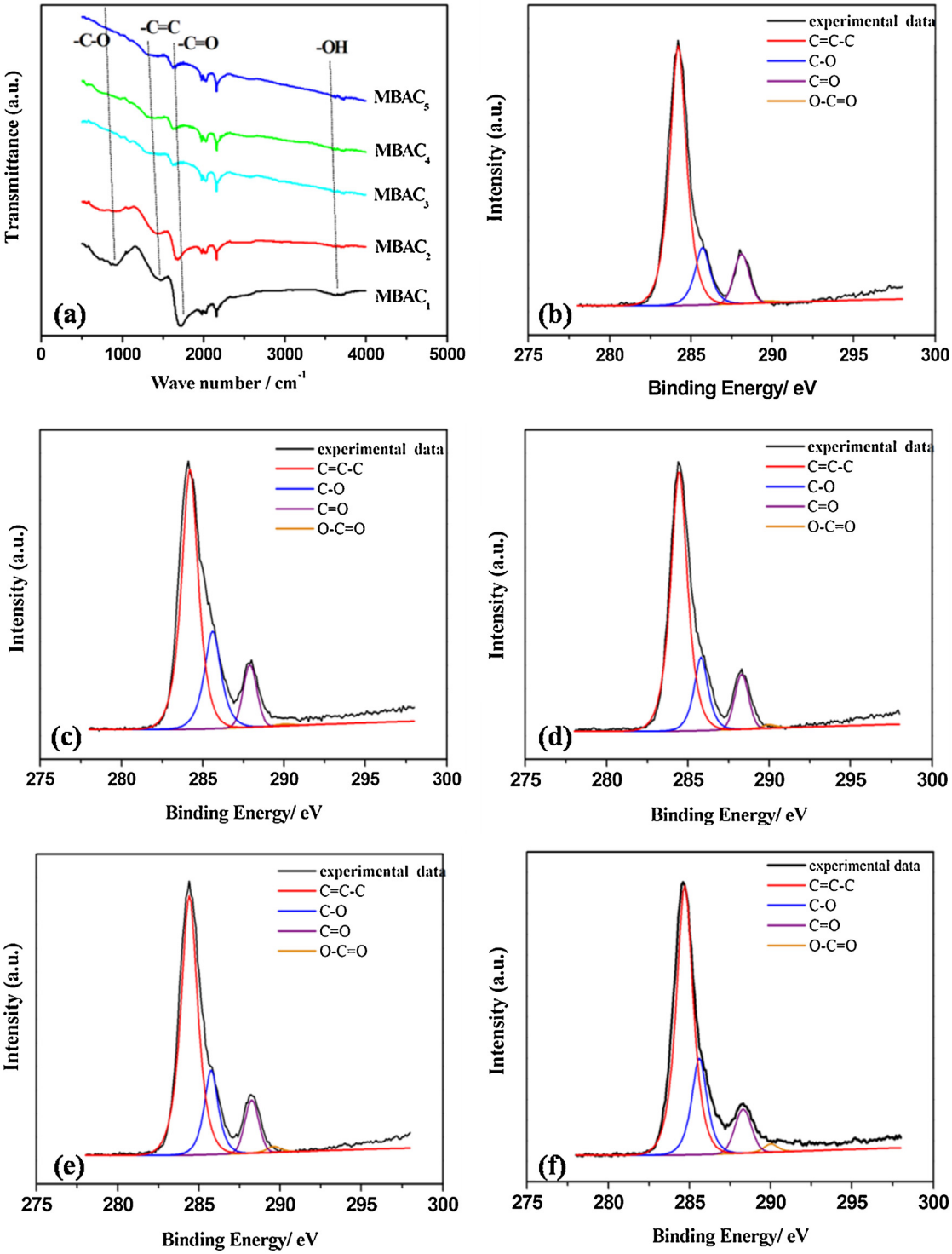

Fig. 3. FTIR spectrum of MBACs (a). High-resolution XPS survey scans of C1s peak for $MBAC_1$ (b), $MBAC_2$ (c), $MBAC_3$ (d), $MBAC_4$ (e), $MBAC_5$ (f).

measurements range from 100 kHz to 10 mHz. All the Nyquist plots can be divided into three parts. The first portion belongs to low frequency region under 0.1 Hz. The virtually upright lines except for $MBAC_1$ in this frequency region illustrate typically capacitive features. The distinction for $MBAC_1$ is mainly caused by its smaller pore size in comparison with other higher temperature activation samples. The second portion lies in the frequency range from 10 to 0.1 Hz, and the slope of curves on Nyquist plots approaches 45°. This region is also named as "knee" range since it's a transitional zone located at the low frequency region (vertical range) and high frequency region (Warburg range). This transitional point between the Warburg range and the vertical range is often known as the

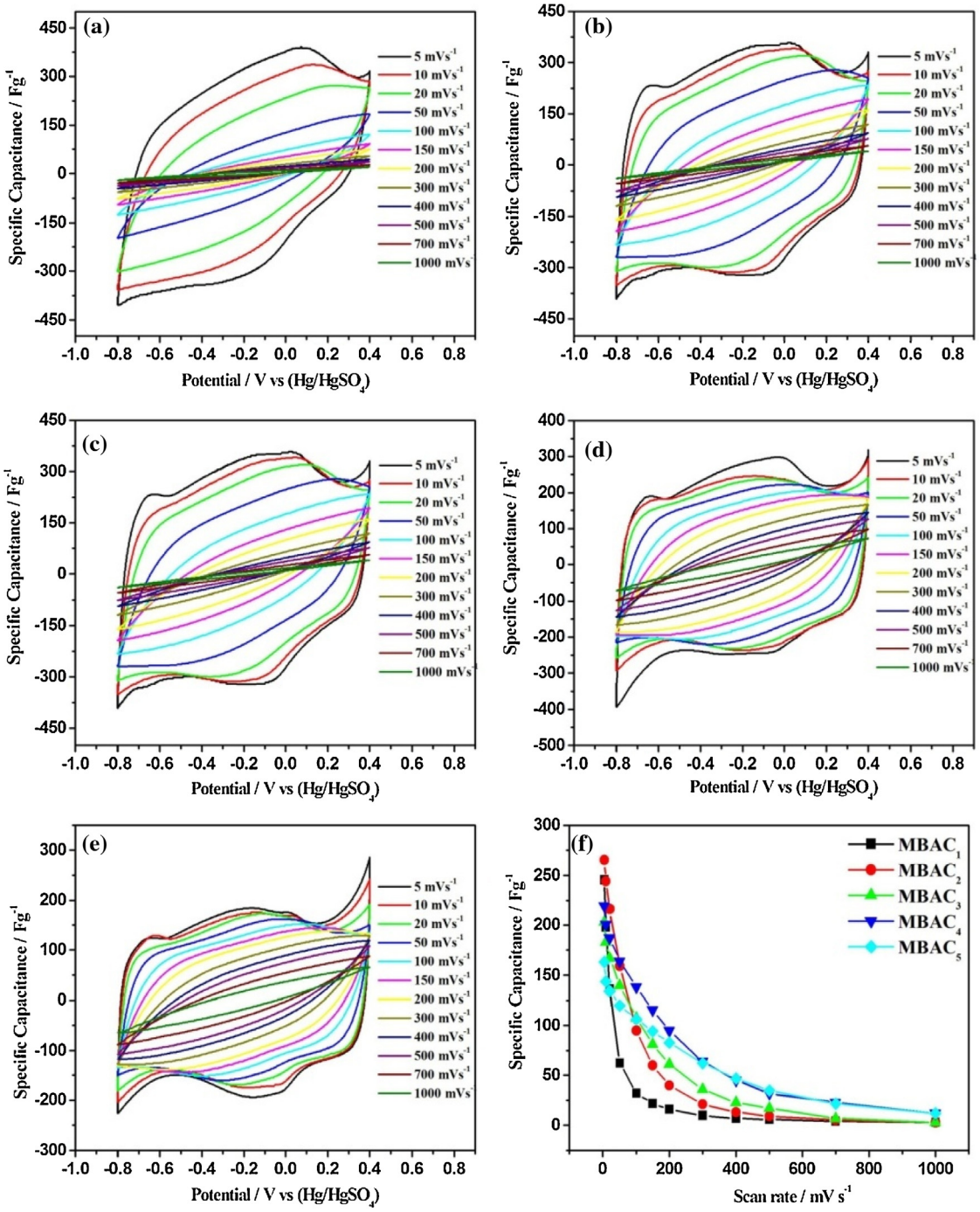

Fig. 4. CV curves of MBAC electrodes at various scan rates in 1 M H_2SO_4 aqueous solutions, respectively (a–e). Calculated SC from the CV measurements at various scan rates (f).

"knee". The frequency at knee suggests the maximum frequency at which capacitive feature is predominate. More important, it is an indication of rate performance for a supercapacitor. Furthermore, the breadth of the cambered impedance in this transitional zone implies the resistance resulted from ion diffusion and transmission at electrode|electrolyte interface. The obvious impedance camber at this range indicates the limited pore size of carbon. The third portion is called as Warburg range. This region generally locates at the interval of 100–100,000 Hz, which is adopted to measure the inner resistance of electrode. It can be deduced that the low inner resistance is caused by high conductivity of acid aqueous solution [45–47]. In addition, the relationships between frequency and two parts of capacitance (real and imaginary) are illustrated in Fig. 5(b) and (c). In the zone of low frequency, the capacitance of real part (C') nearly maintains constancy, which signifies the saturation of capacitance. The capacitance value is remarkably reduced above 0.1 Hz and becoming steady above 10 Hz. The ions in electrolyte can arrive at electrode surface and deeply enter into the pores of the

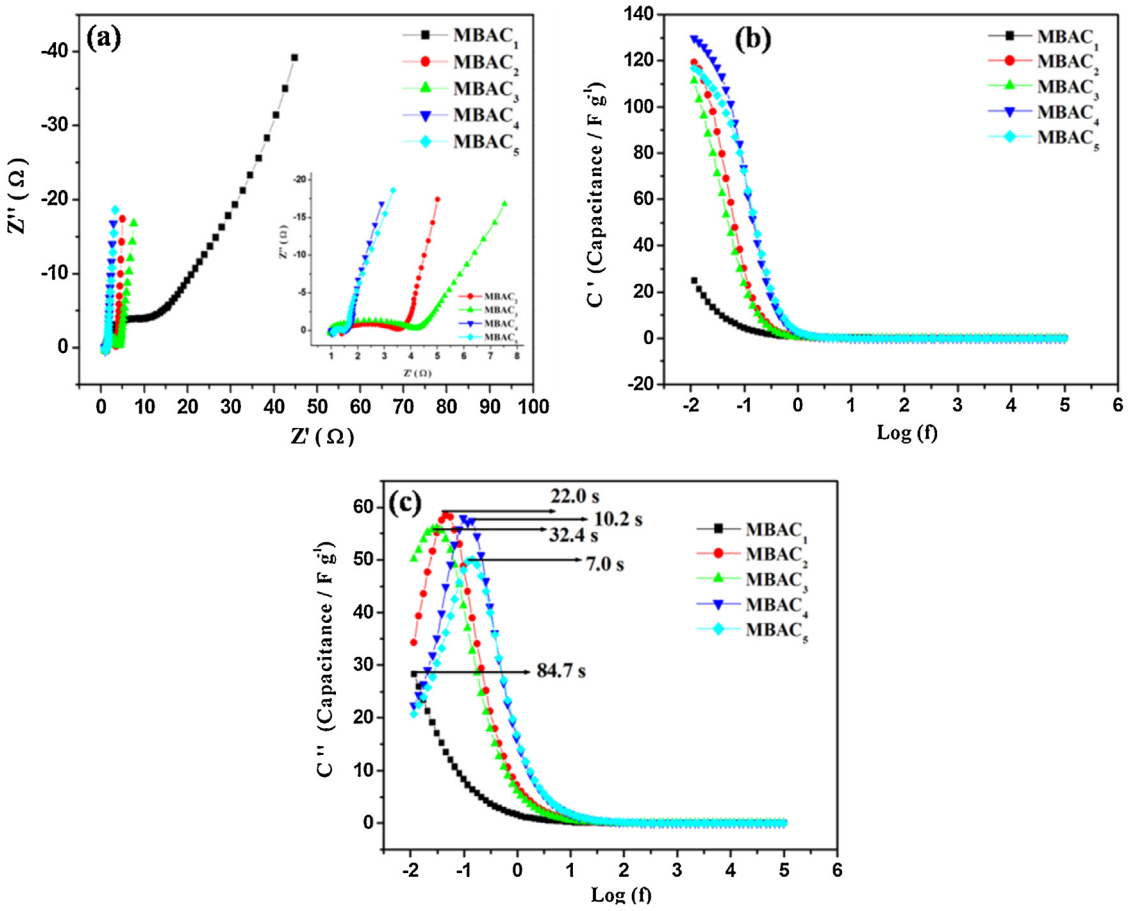

Fig. 5. EIS plots for MBAC electrodes (a). The relationship between frequency and real capacitance plots (b). The relationship between frequency and imaginary capacitance plots (c).

carbon material at low frequency, which finally leads to high capacitance value. However, ions can only arrive at the surface of carbon materials and have little access to deeply penetrating into pores of carbon materials at higher frequency, which results in a rapid reduction in the capacitance. The falling peak in the relationship between frequency and capacitance in imaginary portion implies a max capacitance (C'') at a frequency of f_0. This f_0 also corresponds to a relaxation time τ° ($\tau^\circ = 1/f_0$). The τ° of all MBACs are about 84.7 s, 22.0 s, 32.4 s, 10.2 s, 7.0 s, respectively. This relaxation time is the badly-needed minimum time that the capacitor releases all the energy with an efficiency of above 50% [17,48]. The smaller pore size results in longer relaxation time for low temperature activation samples. This relaxation time also manifests the maximum approachability between the outside surface of the MB-derived carbon material and ions in the electrolyte, which means higher surface area and larger pore size lead to good contact between electrode and electrolyte [49].

Furthermore, GCD was also carried out to assess MBAC's real charge-discharge properties. Firstly, the charge/discharge behaviors of all MBACs at different current densities are demonstrated in Fig. 6(a–e). It is obviously observed that the discharge capacity goes through a remarkable decay with the increase of current density. It also reveals that the $MBAC_2$ shows higher discharge capacity compared with other samples, which is agreed with CV results. The capacity retention in Fig. 6(f) are respectively about 56%, 80%, 73%, 82%, 75% for MBACs when the applied current density is ranged from 0.2 to 2 Ag^{-1}. The fading rate of discharge capacities for $MBAC_2$, $MBAC_3$, $MBAC_4$ and $MBAC_5$ electrodes possesses a slower pace with the enhancement of current density, demonstrating better rate capability, especially for $MBAC_2$ and $MBAC_4$. The specific discharging capacity for $MBAC_2$ slowly reduces from 88 to 70mAhg^{-1} at the current density interval of 0.2 to 2 A g^{-1} and the specific discharging capacity for $MBAC_4$ gradually reduces from 61 to 50 mAh g^{-1} at the same current density interval. These results hints that the as-prepared MBACs exhibit satisfying capacitive performance.

To verify MBAC's practical applications, the symmetrical supercapacitors composed of two MBAC electrodes were fabricated. The full cells for $MBAC_2$, $MBAC_3$ and $MBAC_4$ were respectively assembled and measured. The CVs of capacitors are displayed in Fig. 7(a), which indicates that all capacitors still keep original capacitive behavior and the plump portions at low potential range embody the pseudo-capacitance. The charging and discharging curves of capacitors are exhibited in Fig. 7(b). It can be seen that the charging and discharging curves especially for $MBAC_2$ and $MBAC_3$ have slight deviation from linearity to some degree in acid solution, which illustrates pseudo-capacitance caused by oxygen functional groups makes some contribution to total capacitance. According to the Eqs. (3), (4) and (5), the energy density and power density can be obtained from full-cell charging and discharging curves, which is presented in Fig. 7(c) [50].

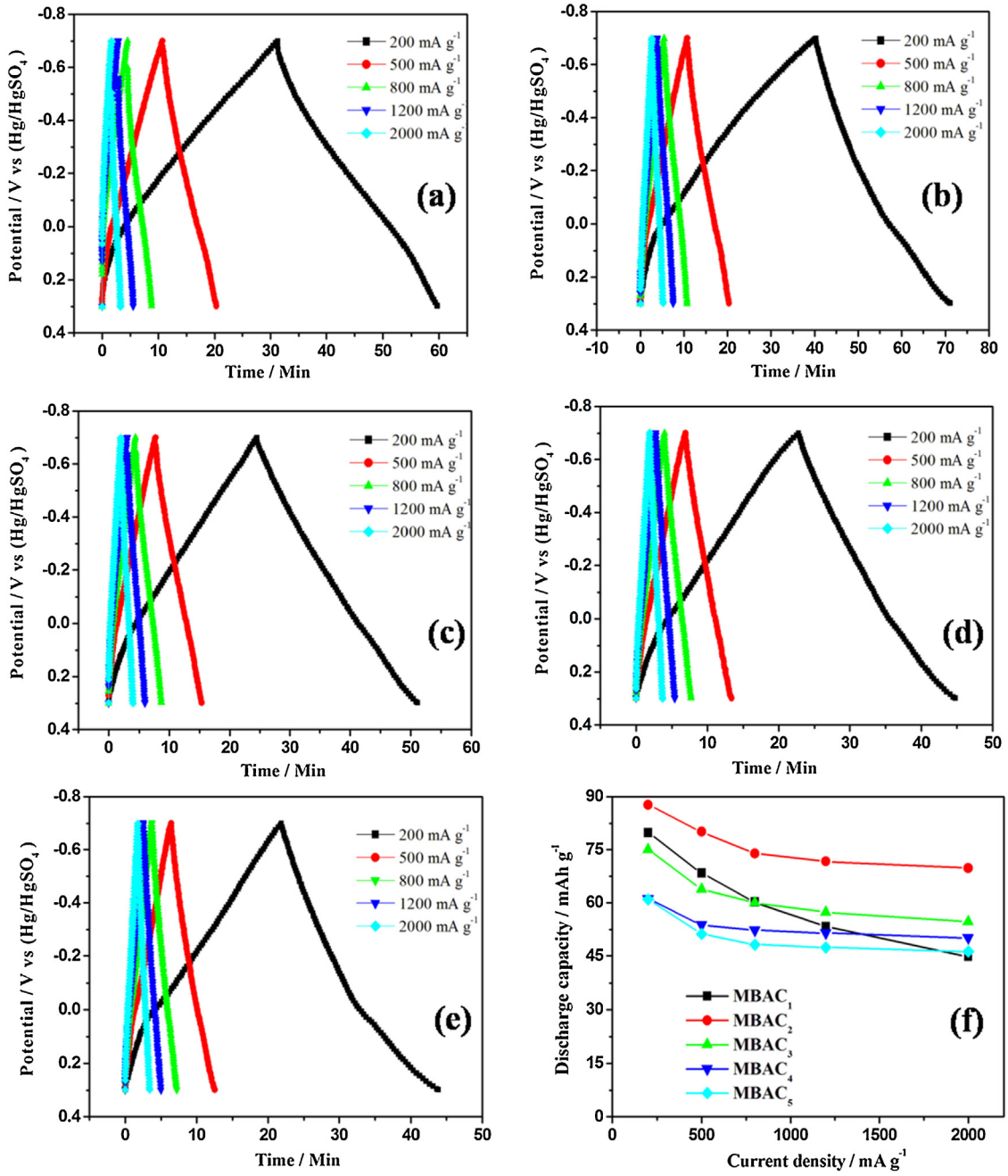

Fig. 6. GCD curves of MBAC electrodes (a–e). The discharge capacity dependent current density (f).

$$E = 0.5CV^2 \tag{3}$$

$$P = \frac{V^2}{4ESR \times m} \tag{4}$$

$$ESR = \frac{\Delta V}{\Delta I} = \frac{\Delta V}{|I_{charge}| + |I_{discharge}|} = \frac{\Delta V}{2I} \tag{5}$$

herein, C represents the specific capacitance of full cell, V stands for the potential window of capacitor, m means the whole weight of active material for both positive and negative electrodes, the equivalent series resistance (ESR) shown in Eq. (5) of a capacitor can be acquired by the IR drop in a complete cycle of charge and discharge. The long term cycling life for MBAC capacitors is also illustrated in Fig. 7(d), which hints that the discharging capacities possess no remarkable declines after 1000 cycles and about 90% of the initial specific capacity is still maintained after 10000 cycle numbers. Meanwhile, the coulombic efficiency can retain about 95% after 10000 long cycles. Hence, the above-discussed performance testifies that this kind of porous carbon displays relative satisfied long-cycling life and long term stability.

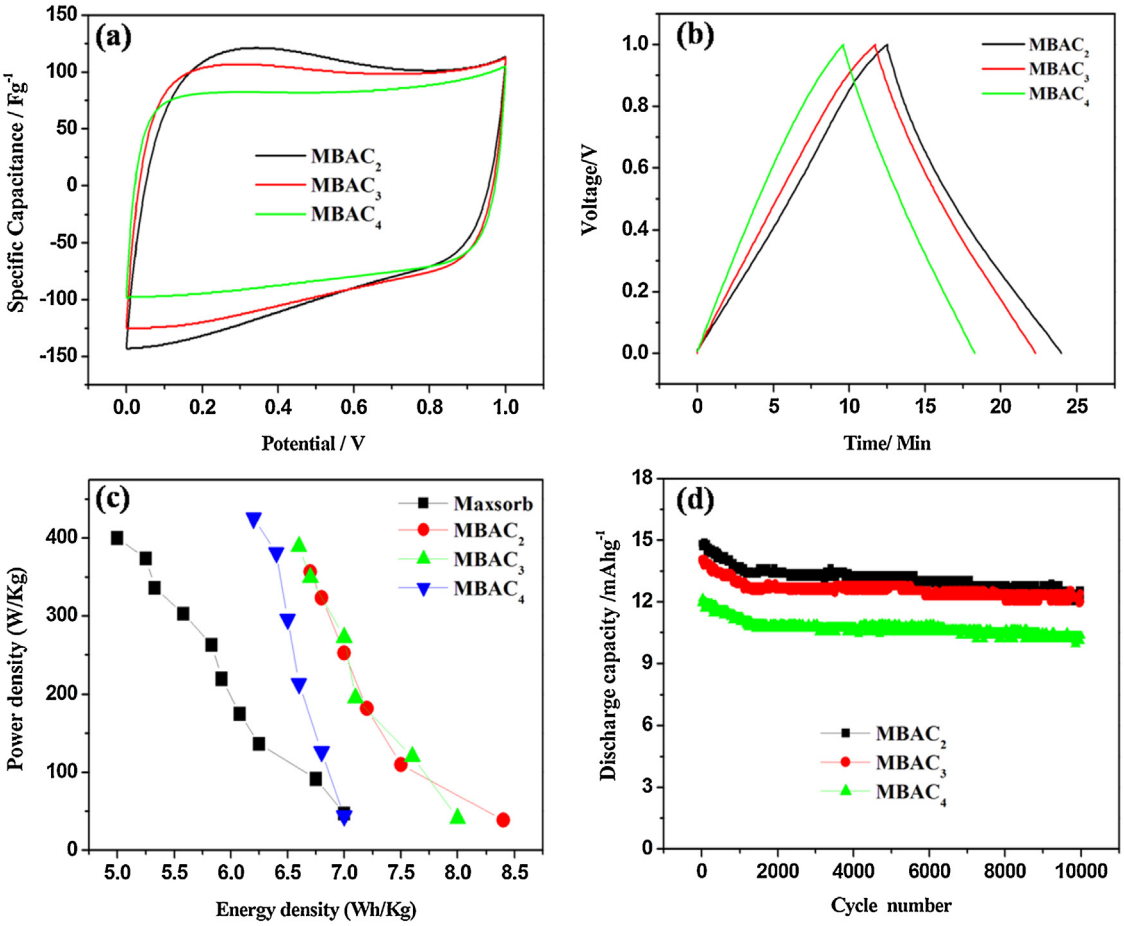

Fig. 7. CVcurves of MBAC capacitors at a scan rate of 20 mV s^{-1} (a). GCD measurments of MBAC capacitors at a current density of 0.2 A g^{-1} (b). The ragone plots of MBAC capacitors (c). The long cycling performance of MBAC capacitors at a current density of 1 A g^{-1} (d).

4. Conclusion

In summary, methylene blue, as one of environmental pollutants, has been reutilized to synthesize porous AC by $ZnCl_2$ activation. The as-prepared ACs have high specific surface area, micro-meso composite pore size and abundant oxygen functional groups, which leads to higher capacitance, good rate performance and desirable long cycle life in acid aqueous electrolytes. Combining their satisfied capacitive response, rational disposal and environmental contamination, MB could be considered as a new carbonaceous precursor to synthesize ACs for high-performance supercapacitors.

Acknowledgment

This project was supported by the National Natural Science Foundation of China (U1303191, 21403295), the “Western Light” Foundation of Chinese Academy of Sciences (XBBS201320), the National Key Technology Research and Development Program of the Ministry of Science and Technology of China (2015BAD14B06).

References

[1] P. Simon, Y. Gogotsi, Materials for electrochemical capacitors, Nature Materials 7 (2008) 845.
[2] X. Zhu, T. Zhao, Z. Nie, Z. Miao, Y. Liu, S. Yao, Nitrogen-doped carbon nanoparticle modulated turn-on fluorescent probes for histidine detection and its imaging in living cells, Nanoscale 8 (2016) 2205.
[3] Y. Wang, Z. Chen, Y. Liu, J. Li, A functional glycoprotein competitive recognition and signal amplification strategy for carbohydrate–protein interaction profiling and cell surface carbohydrate expression evaluation, Nanoscale 5 (2013) 7349.
[4] W. Zhang, L. Wu, Z. Li, Y. Liu, Doped graphene: synthesis, properties and bioanalysis, RSC Advances 5 (2015) 49521.
[5] X. Zhu, T. Zhao, Z. Nie, Y. Liu, S. Yao, Non-redox modulated fluorescence strategy for sensitive and selective ascorbic acid detection with highly photoluminescent nitrogen-doped carbon nanoparticles via solid-state synthesis, Analytical Chemistry 87 (2015) 8524.
[6] Y. He, J. Li, Y. Liu, Reusable and dual-potential responses electrogenerated chemiluminescence biosensor for synchronously cytosensing and dynamic cell surface N-Glycan evaluation, Analytical Chemistry 87 (2015) 9777.
[7] Y. Liu, Y. Liu, H. Feng, Y. Wu, L. Joshi, X. Zeng, J. Li, Layer-by-layer assembly of chemical reduced graphene and carbon nanotubes for sensitive electrochemical immunoassay, Biosensors and Bioelectronics 35 (2012) 63.
[8] W. Qian, F. Sun, Y. Xu, L. Qiu, C. Liu, S. Wang, F. Yan, Human hair-derived carbon flakes for electrochemical supercapacitors, Energy& Environmental Science 7 (2014) 379.
[9] P. Kleszyk, P. Ratajczak, P. Skowron, J. Jagiello, J. Abbas, Q.E. Frackowiak, F. Be'guin, Carbons with narrow pore size distribution prepared by simultaneous carbonization and self-activation of tobacco stems and their application to supercapacitors, Carbon 81 (2015) 148.
[10] J. Zhang, L. Jin, J. Cheng, H. Hu, Hierarchical porous carbons prepared from direct coal liquefaction residue and coal for supercapacitor electrodes, Carbon 55 (2013) 221.
[11] J.E. Zuliani, D.W. Kirk, C.Q. Jia, S. Tong, Activated oil sands fluid coke for electrical double-layer capacitors, Journal of Power Sources 271 (2014) 326.
[12] D. Bhattacharjya, J.S. Yu, Activated carbon made from cow dung as electrode material for electrochemical double layer capacitor, Journal of Power Sources 262 (2014) 224.
[13] C. Peng, X. Yan, R. Wang, J. Lang, Y. Ou, Q. Xue, Promising activated carbons derived from waste tea-leaves and their application in high performance supercapacitors electrodes, Electrochimica Acta 87 (2013) 401.

[14] H. Zhu, J. Yin, X.L. Wang, H. Wang, X.R. Yang, Microorganism-derived heteroatom-doped carbons for oxygen reductions and supercapacitors, Advanced Functional Materials 23 (2013) 1305.
[15] Q. Wang, Q. Cao, X. Wang, B. Jing, H. Kuang, L. Zhou, A high-capacity carbon prepared from renewable chicken feather biopolymer for supercapacitors, Journal of Power Sources 225 (2013) 101.
[16] H. Zhu, X.L. Wang, F. Yang, X.R. Yang, Promising carbons for supercapacitors derived from fungi, Advanced Materials 23 (2011) 2745.
[17] M. Biswal, A. Banerjee, M. Deo, S. Ogale, From dead leaves to high energy density supercapacitors, Energy& Environmental Science 6 (2013) 1249.
[18] K.C. Bedin, A.C. Martins, A.L. Cazetta, O. Pezoti, V.C. Almeida, KOH-activated carbon prepared from sucrose spherical carbon: adsorption equilibrium, kinetic and thermodynamic studies for methylene blue removal, Chemical Engineering Journal 286 (2016) 476.
[19] X. Xin, T. Xu, J. Yin, L. Wang, C. Wang, Management on the location and concentration of Ti^{3+} in anatase TiO_2 for defects-induced visible-light photocatalysis, Applied Catalysis B: Environmental 176 (2015) 354.
[20] R. Kotz, M. Carlen, Principles and applications of electrochemical capacitors, Electrochimica Acta 45 (2000) 2483.
[21] B. Fang, J.H. Kim, M.S. Kim, A. Bonakdarpour, D.P. Wilkinson, J.S. Yu, Fabrication of hollow core carbon spheres with hierarchical nanoarchitecture for ultrahigh electrical charge storage, Journal of Materials Chemistry 22 (2012) 19031.
[22] A. Divyashree, G. Hegde, Activated carbon nanospheres derived from bio-waste materials for supercapacitor applications-a review, RSC Advances 107 (2015) 88339.
[23] G.A. Ali, S.A.B.A. Manaf, A. Kumar, K.F. Chong, G. Hegde, High performance supercapacitor using catalysis free porous carbon nanoparticles, Journal of Physics D: Applied Physics 49 (2014) 495307.
[24] D. Qu, H. Shi, Studies of activated carbons used in double-layer capacitors, Journal of Power Sources 74 (1998) 99.
[25] Y. Zhai, Y. Dou, D. Zhao, Carbon materials for chemical capacitive energy storage, Advanced Materials 23 (2011) 4828.
[26] L.L. Zhang, Y. Gu, X.S. Zhao, Advanced porous carbon electrodes for electrochemical capacitors, Journal of Materials Chemistry A 1 (2013) 9395.
[27] Y. Zhu, S. Murali, M.D. Stoller, K.J. Ganesh, W. Cai, P.J. Ferreira, Carbon-based supercapacitors produced by activation of graphene, Science 332 (2011) 1537.
[28] H.P. Cong, X.C. Ren, P. Wang, S.H. Yu, Macroscopic multifunctional graphene-based hydrogels and aerogels by a metal ion induced self-assembly process, ACS Nano 6 (2012) 2693.
[29] X. He, R. Li, J. Qiu, K. Xie, P. Ling, M. Yu, X. Zhang, M. Zheng, Synthesis of mesoporous carbons for supercapacitors from coal tar pitch by coupling microwave-assisted KOH activation with a MgO template, Carbon 50 (2012) 4911.
[30] S. Murali, D.R. Dreyer, P. Valle-Vigón, M.D. Stoller, Y. Zhu, C. Morales, A.B. Fuertes, C.W. Ruoff, Mesoporous carbon capsules as electrode materials in electrochemical double layer capacitors, Physical Chemistry Chemical Physics 13 (2011) 2652.
[31] Y. Fang, Y. Lv, F. Gong, Z. Wu, X. Li, H. Zhu, D. Zhao, Interface tension-induced synthesis of monodispersed mesoporous carbon hemispheres, Journal of the American Chemical Society 137 (2015) 2808.
[32] G. Wang, Y. Sun, D. Li, H. Liang, R. Dong, X. Feng, K. Müllen, Controlled synthesis of N-doped carbon nanospheres with tailored mesopores through self-assembly of colloidal silica, Angewandte Chemie International Edition 127 (2015) 15406.
[33] S. Feng, W. Li, J. Wang, Y. Song, A.A. Elzatahry, Y. Xia, D. Zhao, Hydrothermal synthesis of ordered mesoporous carbons from a biomass-derived precursor for electrochemical capacitors, Nanoscale 6 (2014) 14657.
[34] J. Ludwinowicz, M. Jaroniec, Effect of activating agents on the development of microporosity in polymeric-based carbon for CO_2 adsorption, Carbon 94 (2015) 673.
[35] J.S. Wei, H. Ding, Y.G. Wang, H.M. Xiong, Hierarchical porous carbon materials with high capacitance derived from schiff-base networks, ACS Applied Materials & Interfaces 7 (2015) 5811.
[36] J.W. Lang, X.B. Yan, W.W. Liu, R.T. Wang, Q.J. Xue, Influence of nitric acid modification of ordered mesoporous carbon materials on their capacitive performances in different aqueous electrolytes, Journal of Power Sources 204 (2012) 220.
[37] G. Milczarek, A. Cizewski, I. Stepniak, Oxygen-doped activated carbon fiber cloth as electrode material for electrochemical capacitor, Journal of Power Sources 196 (2011) 7882.
[38] J.F. Moulder, W.F. Stickle, P.E. Sobel, K.D. Bomben, Handbook of X-ray photoelectron spectroscopy – a reference book of standard spectra for identification and interpretation of XPS data, Perkin-Elmer Corporation, Eden Prairie, MN, USA, 1992.
[39] D. Zhang, J. Yin, J. Zhao, H. Zhu, C. Wang, Adsorption and removal of tetracycline from water by petroleum coke-derived highly porous activated carbon, Journal of Environmental Chemical Engineering 3 (2015) 1504.
[40] C. Moreno-Castilla, M.V. López-Ramón, F. Carrasco-Marín, Changes in surface chemistry of activated carbons by wet oxidation, Carbon 38 (2000) 1995.
[41] J.P. Zheng, T.R. Jow, New charge storage mechanism for electrochemical capacitor, Journal of Electrochemical Society 142 (1995) 6.
[42] J. Yin, D. Zhang, J. Zhao, X. Wang, H. Zhu, C. Wang, Meso- and micro- porous composite carbons derived from humic acid for supercapacitors, Electrochimica Acta 136 (2014) 504.
[43] H. Zhu, X.L. Wang, F. Yang, X.R. Yang, Integrated synthesis to poly (o-phenylenediamine) derived carbons for high performance supercapacitors, Advanced. Materials 24 (2012) 6524.
[44] C. Zheng, L. Qi, M. Yoshio, H. Wang, Cooperation of micro- and meso-porous carbon electrode materials in electric double-layer capacitors, Journal of Power Sources 195 (2010) 4406.
[45] J. Yin, C. Zheng, L. Qi, H. Wang, Concentrated $NaClO_4$ aqueous solutions as promising electrolytes for electric double-layer capacitors, Journal of Power Sources 196 (2011) 4080.
[46] J. Yin, L. Qi, H. Wang, Anti-freezing aqueous electrolytes for electric double-layer capacitors, Electrochimica Acta 88 (2013) 208.
[47] D. Harringtona, A. Driessche, Mechanism and equivalent circuits in electrochemical impedance spectroscopy, Electrochimica Acta 56 (2011) 8005.
[48] P. Taberna, P. Simon, J. Fauvarque, Electrochemical characteristics and iImpedance spectroscopy studies of carbon-carbon supercapacitors, Journal of Electrochemical Society 150 (2003) A292.
[49] D. Pech, M. Brunet, H. Durou, P. Huang, V. Mochalin, Y. Gogotsi, P.L. Taberna, P. Simon, Ultrahigh power electrochemical micro-capacitors based on onion-like carbon, Nature Nanotechnology 5 (2010) 651.
[50] J.E. Zuliani, J.N. Caguiat, D.W. Kirk, C.Q. Jia, Considerations for consistent characterization of electrochemical double-layer capacitor performance, Journal of Power Sources 290 (2015) 136.